# Enhanced Tumor Treatment Using Biofunctional Indocyanine Green-Containing Nanostructure by Intratumoral or Intravenous Injection

Xiaohui Zheng,[†,‡] Feifan Zhou,[†,‡] Baoyan Wu,[†] Wei R. Chen,[†,§] and Da Xing*[,†,‡]

[†]MOE Key Laboratory of Laser Life Science & Institute of Laser Life Science, College of Biophotonics, and [‡]Joint Laboratory of Laser Oncology with Cancer Center of Sun Yat-Sen University, South China Normal University, Guangzhou 510631, China
[§]Department of Engineering and Physics, College of Mathematics and Science, University of Central Oklahoma, Edmond, Oklahoma 73034, United States
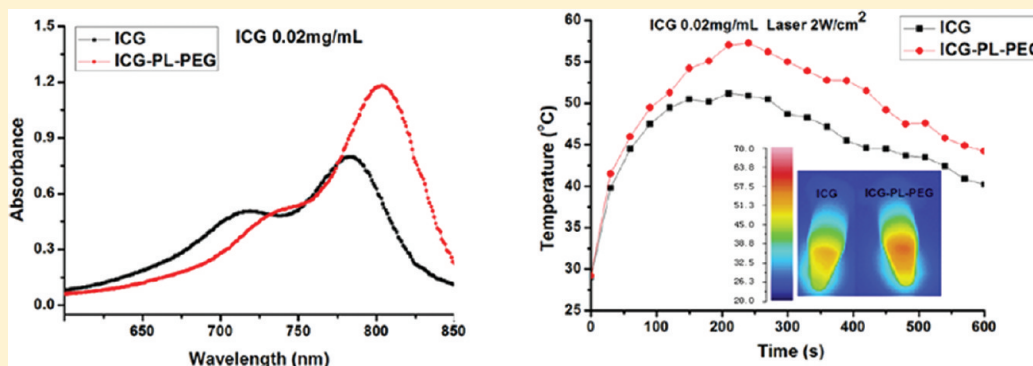
ABSTRACT: Indocyanine green (ICG) is a conventional dye that can be used in clinical near-infrared (NIR) imaging, and it is also an effective light absorber for laser-mediated photothermal therapy. However, applications of ICG were limited due to its fast degradation in aqueous media and quick clearance from the body. Herein, an ICG-containing nanostructure, ICG-PL-PEG, was developed for photothermal therapy, which was self-assembled by ICG and phospholipid-polyethylene glycol (PL-PEG). Our *in vitro* and *in vivo* experiments demonstrated that ICG-PL-PEG suspension was more efficient in producing a NIR-dependent temperature increase than ICG alone, due to the increase of ICG monomers from the addition of PL-PEG to match the central wavelength of the 808 nm laser. When conjugated with integrin $\alpha_v\beta_3$ monoclonal antibody (mAb), ICG-PL-PEG could be selectively internalized and retained in target tumor cells. Irradiation of an 808 nm laser after intravenous administration of ICG-PL-PEG-mAb resulted in tumor suppression in mice, while ICG alone had only limited effect. This is the first time an ICG-containing nanostructure has been used through systemic administration to achieve an efficient *in vivo* photothermal effect for cancer treatment. Therefore, ICG-PL-PEG could be used as a fluorescent marker as well as a light-absorber for imaging-guided photothermal therapy. All the components of ICG-PL-PEG have been approved for human use. Therefore, this unique ICG-containing nanostructure has great potential in clinical applications.

KEYWORDS: *laser-mediated photothermal therapy, ICG-containing nanostructure, self-assembly, NIR-dependent temperature increase, photothermal tumor suppression*

INTRODUCTION

Photothermal therapy for cancer has been widely investigated as an effective local, minimally invasive treatment modality in comparison with other methods,[1,2] due to its precise energy delivery to target tissue and the sensitivity of tumor tissue to temperature increase.[3] Light in the near-infrared (NIR) region, in combination with appropriate light-absorbing agents, is particularly attractive for selective photothermal interaction, because of the low absorbance of biological tissue in this region.[4] Recently, nanotechnology has engendered a range of novel materials acting as photothermal agents, including gold nanomaterials (gold nanocage, gold nanoshell and gold nanorod)[5−9] and carbon nanomaterials (grapheme, nanohorns, and single-walled and multiwalled carbon nanotubes).[10−14]

Despite recent progress, these nanoparticles have not been used in clinical applications due to the concerns of their long-term safety.[15] Recently, much attention has been focused on the development of nanostructure with integrated imaging and therapeutic functions. A new term "nanotheranostics" has been proposed to describe these nanoparticles.[16−18] Though gold and carbon nanomaterials can be used in photothermal therapy, they have not been used in disease detection. Targeted drug delivery or imaging-guided drug delivery using these nanoparticles, especially gold nanomaterials, has been limited due to

their low drug loading efficiency.[19] In contrast, organic nanoparticles, such as liposomes, micelles, and polymersomes, have been applied in human studies due to their biocompatibility and drug-delivery capacity.[20] However, as these organic nanoparticles do not absorb or emit light in the near-infrared region, they have been limited for NIR optical imaging and photothermal therapy.[21] Therefore, development of nanostructures with both drug delivery properties and excellent NIR optical properties is needed.

Indocyanine green (ICG) is a U.S. Federal Drug Administration approved NIR clinical imaging agent,[22−24] and it is also an effective NIR light absorber for laser-mediated photothermal therapy.[25−29] Therefore, ICG is a suitable candidate for dual-functional probes integrating NIR fluorescence imaging and photothermal therapeutic properties. Use of ICG in NIR fluorescence imaging has been studied intensely.[30−34] However, as a strong light-absorber, application of ICG in photothermal therapy has not been thoroughly explored,[35−37] due to its fast degradation in aqueous media and quick clearance from the body.[24,38−40] Polymeric modalities have been used to address the intrinsic drawbacks of ICG.[30,32−34,41−45] Among these modalities, micelles are a successful drug delivery system and have provided ICG with good stability.[32,45] However, these ICG-containing nanostructures have been only tested in imaging and their photothermal therapeutic effects have not been explored.

Previously, ICG has been used as a photothermal chromophore for tumor treatment through intratumoral injection.[25−27] To further explore ICG for both disease imaging/detection and photothermal therapy, we have constructed ICG-PL-PEG, an ICG containing nanostructure self-assembled by ICG and PL-PEG, as a NIR dual-functional targeting probe for optical imaging and photothermal therapy.[46] The limitations of ICG applications due to concentration-dependent aggregation, poor aqueous stability and lack of target specificity could be overcome using this new nanostructure. In the current work, photothermal properties of ICG-PL-PEG were further investigated. The enhancement of tumor treatment using ICG-PL-PEG, administered intratumorally or intravenously, followed by irradiation of NIR light, was observed.

Our *in vitro* and *in vivo* experiments demonstrated that ICG-PL-PEG suspension was more efficient in producing a NIR-dependent temperature increase than ICG alone, due to the increase of ICG monomers from the addition of PL-PEG to match the central wavelength of the 808 nm laser. When conjugated with integrin $\alpha_v\beta_3$ monoclonal antibody (mAb), ICG-PL-PEG could be selectively internalized and retained in target tumor cells. Irradiation of an 808 nm laser after intravenous administration of ICG-PL-PEG-mAb resulted in tumor suppression in mice, while ICG alone had only limited effect. To the best of our knowledge, this is the first time an ICG-containing nanostructure has been used through systemic administration to achieve an efficient *in vivo* photothermal effect for cancer treatment.

■ EXPERIMENTAL SECTION

The following chemicals and reagents were used in our experiments: 1,2-distearoyl-*sn*-glycero-3-phosphoethanolamine-*N*-[carboxy(polyethylene glycol)-2000] (PL-PEG-COOH) (Avanti Polar Lipids Inc., Mt. Eden, AL, USA), indocyanine green for injection (Sigma Chemical Co., St. Louis, MO), integrin $\alpha_v\beta_3$ (23C6) monoclonal antibody (integrin $\alpha_v\beta_3$ mAb) (Santa Cruz, CA, USA), FITC (Sigma Chemical Co., St. Louis, MO), *N*-hydroxysulfosuccinimide (NHS), and 1-ethyl-3-(3-(dimethylamino)propyl)carbodiimide (EDC) (Sigma-Aldrich Co). Since all the reagents were of analytical grade, they were used without further purification.

Preparation of ICG-PL-PEG and ICG-PL-PEG-mAb Formulations. Indocyanine green containing nanostructure (ICG-PL-PEG) was prepared following the procedures as previously described.[46] Briefly, ICG and PL-PEG were mixed with a mass ratio of 1:100. The solution was stirred at room temperature for 5 min and was filtrated using 2000 Da filters (Millipore) to remove excess nonbinding ICG. For ICG-PL-PEG-mAb, PL-PEG-COOH solution was first activated by EDC/NHS to afford PL-PEG-NHS (molar ratio, PL-PEG:EDC:NHS = 1:2:2). After reaction, the solution was dialyzed against PBS using a 2000 Da membrane (Millipore) to remove excess EDC and NHS. To ensure complete removal, the dialysis lasted 3 to 4 days with frequent replacement of PBS buffer. ICG-PL-PEG-mAb was produced by incubating integrin $\alpha_v\beta_3$ monoclonal antibody with ICG-PL-PEG-NHS (molar ratio, PL-PEG-NHS:integrin $\alpha_v\beta_3$ monoclonal antibody = 200:1) (pH 7.4) for 4 h.

Fluorescence Labeling of ICG-PL-PEG-mAb. Integrin $\alpha_v\beta_3$ mAb was first labeled with FITC by the procedures according to Ou.[47] Briefly, the solution of integrin $\alpha_v\beta_3$ mAb at a concentration of 40 nM in standard PBS was mixed with 50 μL of sodium bicarbonate solution. The solution was then mixed with FITC (13 mM, 100 μL) dissolved in DMSO (Aldrich). After incubating the mixture for 1 h at room temperature, protected from illumination, the conjugated integrin $\alpha_v\beta_3$ mAb−FITC was filtrated through 100 kDa filters (Millipore) to remove excess FITC. The resultant fluorescein labeled protein solution was then diluted with PBS to a concentration of 8 nM. FITC labeled integrin $\alpha_v\beta_3$ was then used to produce ICG-PL-PEG-mAb/FITC. If fluorescence emissions from both ICG and FITC were present in target cancer cells (U87-MG) while absent in nontarget cells (MCF-7), it provided evidence that ICG-PL-PEG-mAb/FITC remained a stable structure after entering target cells.

Optical Spectra Measurements. The absorption spectra of freely dissolved ICG and ICG-PL-PEG probe were obtained using a UV/vis spectrometer (Lambda 35, Perkin-Elmer, USA).

***In Vitro* Study of ICG-PL-PEG-mAb.** Experiments were performed according to our previous protocol.[46] Briefly, two types of cancer cells (U87-MG and MCF-7) growing in 35 mm Petri dishes were incubated with ICG-PL-PEG-mAb/FITC formulation at 0.01 mg/mL ICG (mass ratio ICG:PL-PEG = 1:100) for 1 h, rinsed with PBS and replaced with fresh cell medium. The cells were imaged by a laser scanning microscope.

Confocal Laser Scanning Microscopy. Fluorescence emissions from FITC and ICG were observed confocally using a commercial laser scanning microscope (LSM 510 META) combination system (Zeiss, Jena, Germany) equipped with a Plan-Neofluar 40×/1.3 NA Oil DIC objective. Excitation wavelength and detection filter settings for each of the fluorescent indicators were as follows. FITC was excited at 488 nm with an Ar ion laser (reflected by a beam splitter HFT 488 nm), and the fluorescence emission was recorded through a 500−550 nm IR band-pass filter. ICG was excited at 633 nm with a He−Ne laser, and emitted light was recorded through a 650 nm long-pass filter.

Cell Lines and Animal Model. NIR photothermal therapy was an attractive treatment modality for cancer. Based on

previous study, ICG has been used to effectively suppress rat mammary tumors under laser irradiation.[25−27] Murine mammary tumor line EMT6 was selected to generate breast cancer. U87-MG human glioblastoma cancer cells and MCF-7 human breast cancer cells were selected to match ICG-PL-PEG-mAb, according to our previous protocol.[46] U87-MG cancer cells overexpress integrin $\alpha_v\beta_3$ on the cell surface,[48] while MCF-7 cancer cells express a very low level of integrin $\alpha_v\beta_3$. Murine mammary tumor line EMT6 cells were cultured in RPMI 1640 (GIBCO) supplemented with 15% fetal bovine serum (FBS), penicillin (100 units/mL), and streptomycin (100 μg/mL) in 5% CO_2, 95% air at 37 °C in a humidified incubator. U87-MG cells and MCF-7 cells were cultured in Eagle's minimal essential medium (EMEM) and Dulbecco's modified Eagle's medium (DMEM), respectively. The media were supplemented with 10% fetal bovine serum (FBS) and 1% penicillin−streptomycin in 5% CO_2, 95% air at 37 °C in a humidified incubator. For in situ intratumoral injection experiment, EMT6 cells (1×10^6) in 100 μL of PBS solution were injected into the flank region of female Balb/c mice, aged 6−8 weeks. Animals were used in experiments 7 to 10 days after tumor cell inoculation, when the tumors reached a size of approximately 300 mm³. For intravenous injection experiment, the U87-MG tumors were generated by subcutaneous injection of 1×10^7 cells in 100 μL of PBS to female athymic nude mice. Animals used in photothermal studies had a tumor volume of 200−400 mm³. Tumor sizes were measured by a caliper every other day, and the tumor volume was calculated as volume = (tumor length) $\times$ (tumor width)²/2. Relative tumor volumes were calculated as V/V_0 (V_0 was the tumor volume at the time when the tumor was treated by laser irradiation).

***In Vivo* Study of ICG-PL-PEG-mAb and Biodistribution.** Nine nude mice bearing U87-MG tumor were randomly divided into three groups ($n = 3$ per group). Mice in group 1 were intravenously injected via tail vein with 100 μL of PBS as control. Mice in groups 2 and 3 were intravenously injected with 200 μL of ICG and ICG-PL-PEG-mAb, respectively (both containing 0.1 mg/mL ICG). Six hours later, mice bearing U87-MG tumors were imaged. Then various organs and tissues were obtained for imaging and semiquantitative biodistribution analysis. Detection was performed using the LI-COR Odyssey Infrared Imaging System through 800 nm channel (LI-COR, Inc. Lincoln, NE).

Temperature Measurement and Photothermal Therapy during NIR Irradiation. For *in vitro* experiments, ICG and ICG-PL-PEG solutions (0.02 mg/mL ICG, 500 μL) in tubes were irradiated by the 808 nm laser (COHERENT 899-05, USA) at 2.0 W/cm² for 10 min. Temperature was measured in 5 s intervals with an infrared thermal camera (TVS200EX, NEC, Japan). For *in situ* intratumoral injection experiment, 6 female Balb/c mice bearing EMT6 tumors were randomly divided into two groups ($n = 3$ per group). In group 1, mouse tumors were injected with 100 μL of PBS as control, while in group 2, mouse tumors were injected with 100 μL of ICG (left tumor) and ICG-PL-PEG (right tumor) formulation (both containing 0.5% ICG). Both tumors were irradiated by the 808 nm laser at 0.5 W/cm² 3 h postinjection for 100 s, and surface temperatures of the tumors were measured in 5 s intervals with the infrared thermal camera. Three hours was selected for ICG to diffuse through the entire tumor. For intravenous injection experiment, 9 nude mice bearing U87-MG tumors were randomly divided into 3 groups ($n = 3$ per group). The mice in group 1 were intravenously injected via tail vein with 100 μL

of PBS as control. The mice in groups 2 and 3 were intravenously injected with 100 μL of ICG and ICG-PL-PEG-mAb, both containing 0.5% ICG (a dose of 25 mg/kg). Six hours later, mice in all groups were treated by the 808 nm laser with 2 W/cm² for 10 min. All the experiments were conducted at room temperature.

Different Intensities and Exposure Times. To select laser intensity, we performed a pre-experiment of skin irradiation with laser power densities from 0.5 to 2.0 W/cm² (data not shown). There was no apparent damage on the mouse skin under laser irradiation below 2.0 W/cm². Therefore, 2.0 W/cm² was selected as the maximum dose in our experiments. For spot size, the laser beam was adjusted to cover the entire tumor (120.7−158.8 mm²). Different exposure times were used for *in vitro*, *in situ*, and intravenous studies.

■ RESULTS

ICG-PL-PEG Suspension Was More Efficient in Producing a NIR-Dependent Temperature Increase than ICG *in Vitro* and *in Vivo*. ICG-containing nanostructure (ICG-PL-PEG) was prepared following our previous protocol.[46] The average diameter of ICG-PL-PEG was 17.6 nm, which was demonstrated by dynamic light scattering in our previous study.[46] The data obtained by TEM was also within the range. After conjugation with integrin $\alpha_v\beta_3$, the average diameter changed to 21.5 nm (data not shown). Compared to ICG, the peak absorbance of ICG-PL-PEG was red-shifted from 780 to 800 nm to match the central wavelength of the diode laser (808 nm) and the absorbance had an apparent increase at this wavelength (Figure 1A).

To verify the potential of using ICG and ICG-PL-PEG in photothermal therapy, we monitored the temperature increase *in vitro* during laser irradiation using an infrared camera. Both ICG and ICG-PL-PEG (with the same concentration of ICG) were exposed to an 808 nm NIR laser at a power density of 2 W/cm² for 10 min, and both showed a rapid increase of temperature. At an ICG concentration of 0.02 mg/mL, ICG-PL-PEG had a temperature elevation up to 57.3 °C, while the ICG aqueous solution had a temperature elevation only to 50.5 °C. Due to photodegradation and thermal degradation, there was a slow temperature decline after 4 min (Figure 1B). These findings clearly demonstrated that the absorption of light could be converted to heat and the ICG-PL-PEG formulation had a greater temperature increase than ICG solution in response to NIR illumination.

To further confirm this conclusion, we carried out an intratumoral injection experiment to investigate the photothermal effects of ICG and ICG-PL-PEG using mice with bilateral tumors (on the left and right flanks). Solutions of 100 μL of ICG and ICG-PL-PEG containing 0.5% ICG were injected into the center of each tumor (Figure 2A) (following the procedure as previously described).[25−27] The tumors on each mouse were subjected to photothermal treatment by exposure to the 808 nm diode laser at a power density of 0.5 W/cm². During the laser treatment, full-body thermographic images were captured using an infrared camera, as shown in Figures 2B and 2C. The maximum average temperature of the tumor surface was plotted as a function of the irradiation time (Figures 2D and 2E). Without ICG or ICG-PL-PEG injection, the tumors on the left and right have similar photothermal response under the 808 nm laser irradiation. Three hours postinjection, the surface temperature of the right tumor injected with ICG-PL-PEG increased rapidly within 100 s and

A)

B)
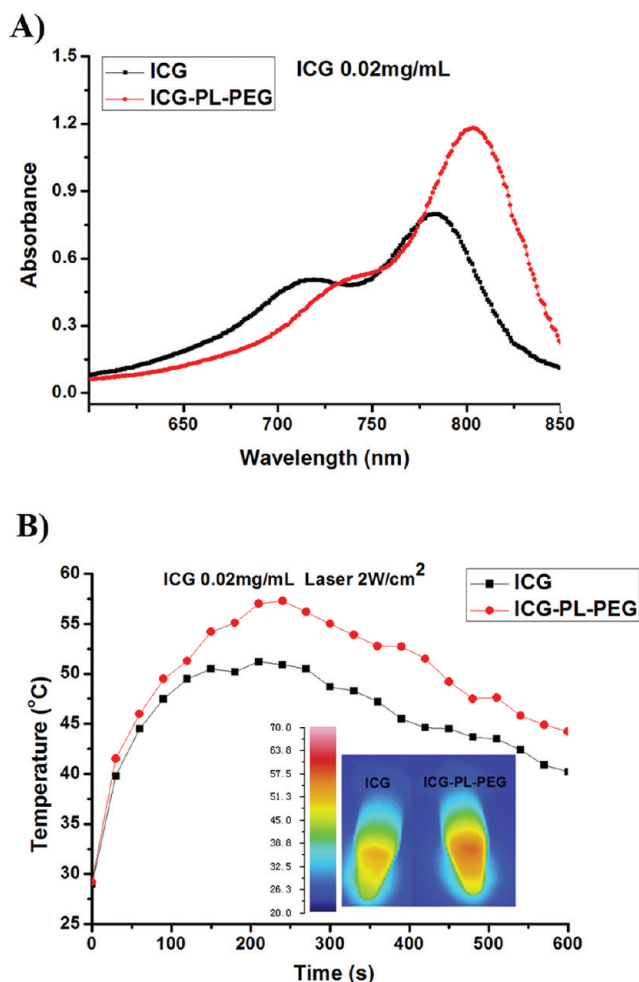
Figure 1. Absorption spectra and temperature increases of ICG and ICG-PL-PEG. (A) UV−vis-NIR absorption spectra of ICG and ICG-PL-PEG. (B) Temperature increases in ICG or ICG-PL-PEG formulation in response to irradiation of an 808 nm laser with a power density of 2 W/cm^2 and a duration of 10 min. Inset: thermographic images of ICG and ICG-PL-PEG in vials after laser irradiation for 4 min.

reached about 60 °C. The surface temperature of the left tumor injected with ICG reached only about 50 °C.

Targeting of ICG-PL-PEG-mAb *in Vitro* and *in Vivo*. Our previous work demonstrated that ICG-PL-PEG-mAb could be used as efficient and selective photothermal absorbers to destroy cancer cells with a near-infrared laser.[46] In our experiments, ICG-PL-PEG-mAb was further labeled by FITC (abbreviated as ICG-PL-PEG-mAb/FITC). The fluorescence emissions of both ICG (red) and FITC (green) were colocalized in U87-MG cancer cells (Figure 3). Strong fluorescence emissions from both ICG and FITC were present in target cancer cells while absent in nontarget cells, indicating that ICG-PL-PEG-mAb/FITC remained a stable structure after entering target cells.

Further, the *in vivo* biodistribution of ICG and ICG-PL-PEG-mAb was assessed for animal whole body NIR imaging, using PBS, ICG and ICG-PL-PEG-mAb. The whole body NIR fluorescent images of mice were obtained six hours after intravenous injection, using the LI-COR Odyssey Infrared Imaging System through 800 nm channel (LI-COR, Inc. Lincoln, NE). ICG was found to be mainly accumulated in

liver, while ICG-PL-PEG-mAb had a high accumulation in both tumor and liver (Figure 4A). Therefore, ICG-PL-PEG could be used as a fluorescent marker as well as a light absorber for imaging-guided photothermal therapy. Then the mice were sacrificed and various organs and tissues were collected for imaging analysis (Figure 4B). The averaged ICG fluorescent intensity of each imaged organ (after removing the tissue autofluorescence and subtracting the background) was calculated for a semiquantitative biodistribution analysis. The strongest fluorescence signal of ICG was observed in the liver while it was in tumor for ICG-PL-PEG-mAb (4.7-fold of free ICG, *P* < 0.001), suggesting a high tumor accumulation of ICG-PL-PEG-mAb in tumor. An obvious trend of increased fluorescence signal was obtained in most major organs for ICG-PL-PEG-mAb (Figure 4C), suggesting different metabolic characteristics between ICG and ICG-PL-PEG-mAb.

Photothermal Treatment of Tumors Using Laser Irradiation Following Intravenous Administration of ICG and ICG-PL-PEG-mAb. Motivated by the tumor accumulation of ICG-PL-PEG-mAb and its strong NIR optical absorption ability at 808 nm, we further carried out an *in vivo* photothermal therapy study using the U87-MG tumor model on athymic nude mice. Solutions of ICG and ICG-PL-PEG-mAb (100 μL; 0.5% ICG) were intravenously injected via tail vein (Figure 5A). After 6 h, the tumors on each mouse in different groups were treated by the 808 nm diode laser at a power density of 2W/cm^2 for 10 min (Figure 5B).

During photothermal treatment, full-body thermographic images were captured using an infrared camera. The maximum surface temperature of the tumor area was plotted as a function of the irradiation time. For the ICG injected mice, the tumor surface temperature increased rapidly within 100 s and began to plateau at about 45 °C. For the ICG-PL-PEG-mAb injected mice, tumor surface temperature rapidly reached 55 °C. The surface of the tumor treated by laser only had a temperature plateau of 40 °C (Figure 5C).

Photothermal damage to tumor cells in mice intravenously injected with PBS, ICG and ICG-PL-PEG-mAb was confirmed by histological examination using H&E staining, 12 h after photothermal treatment. Distinctive characteristics of cellular damage, including coagulative necrosis, abundant pyknosis and considerable regions of karyolysis, were found in laser-treated tumor tissue from mice injected with ICG-PL-PEG-mAb; but the damage was largely absent from tumors injected with PBS or ICG (Figure 5D). From the Arrhenius integral, laser induced thermal damage increases at a constant rate when tissue temperature is held constant. However, for linearly increasing temperatures, the rate of increase in damage is exponential, suggesting an accelerated rate of thermal damage to tissue that is almost instantaneous.[49] A 10 degree increase in temperature can make a substantial difference in photothermal therapy.

After treatment, mice were observed daily and the tumor volumes were measured using a caliper every other day. The mice treated by laser + ICG had an average tumor burden similar to that of control mice (laser + PBS). In contrast, laser + ICG-PL-PEG-mAb treatment (2 W/cm^2 for 10 min) caused significant tumor suppression (Figure 5E).

■ **DISCUSSION**

Generally, NIR absorption cross section of gold nanoparticles, such as nanorod, nanoshell, and nanocage, is 10^4−10^6-fold higher than that of conventional organic dyes.[5,6] However, based on optical absorption per mass, the absorption efficiency
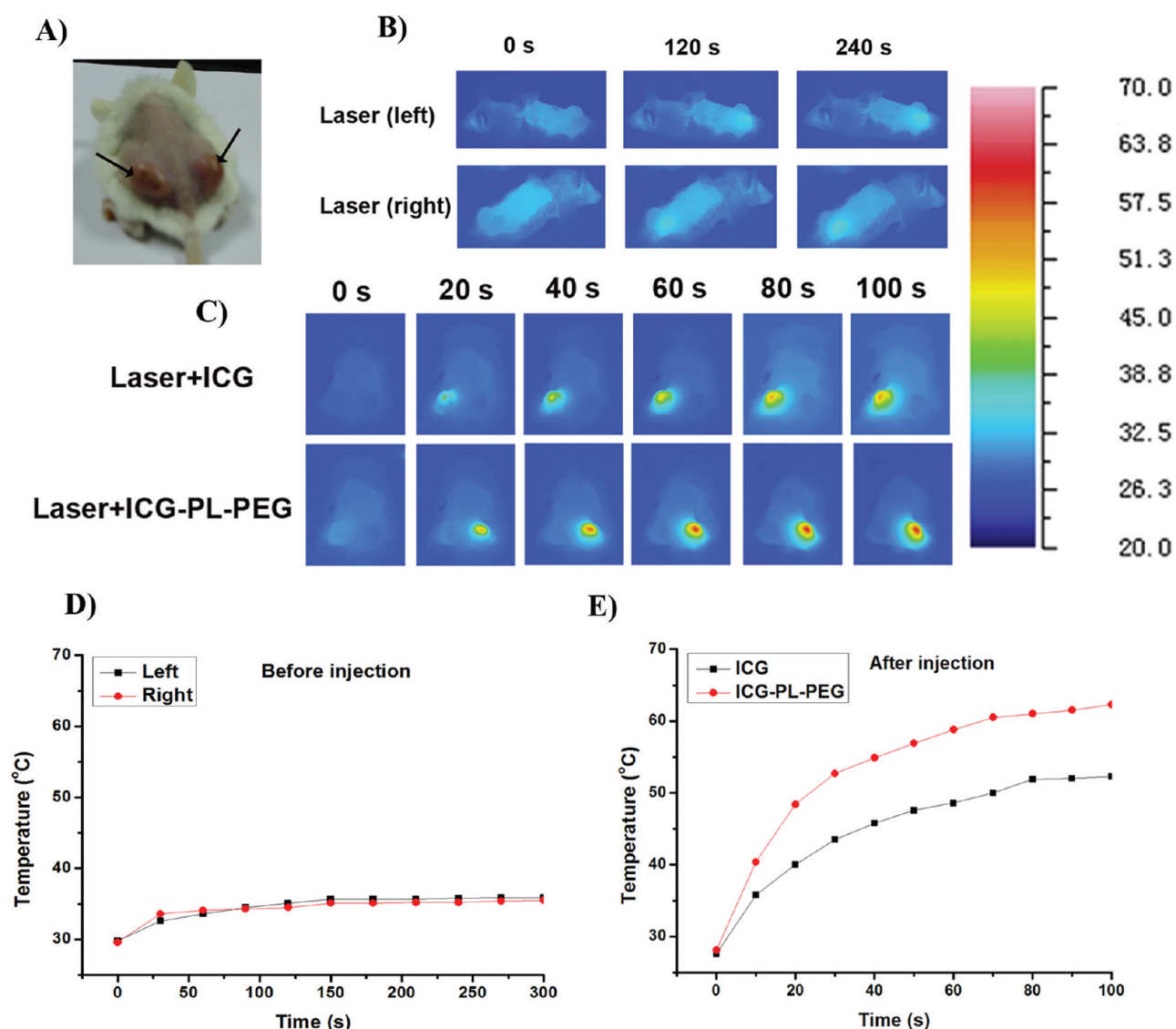
Figure 2. Temperature increase in tumor tissue with or without ICG or ICG-PL-PEG in response to irradiation of an 808 nm laser with a power density of 0.5 W/cm^2 and different durations. (A) Photograph of a mouse bearing bilateral tumors. (B, D) Thermographic image and plots of average temperature increase of bilateral tumors during 808 nm laser irradiation without ICG or ICG-PL-PEG. (C, E) Thermographic image and plots of average temperature increase of bilateral tumors during 808 nm laser irradiation 3 h after injection of ICG (left tumor) and ICG-PL-PEG (right tumor).

of ICG is about 8500 times more than that of commercial gold nanorods with peak absorption at 780 nm and 7 times more than SWNTs.[50] The effective dose of ICG-PL-PEG used in our experiments (25 mg/kg) was much lower than the maximum dose (LD$_{50}$) of ICG alone (50−80 mg/kg).[30] This lays the foundation for using ICG in photothermal therapy based on the following. (1) The major advantage of ICG in selective photothermal therapy lies in its absorption spectrum. ICG absorbs strongly and also fluoresces in the near-infrared region, to which biological tissue is relatively transparent. (2) Intratumoral injection of ICG has been used in photothermal therapy in animal studies, and it could effectively suppress tumor growth .[25−27] (3) ICG is currently approved by FDA as a NIR clinical imaging agent. However, it has been allowed to be used in clinical trials for laser treatment of melanoma patients since 2004 in the US.[51,52] Furthermore, ICG has been used for its photothermal effect in breast cancer treatment in clinical trials outside the US.[53] These clinical and preclinical results

show that ICG is a nontoxic, efficient light-absorbing dye and holds great promise for selective photothermal therapy. Our current work should further advance the therapeutic use of ICG for cancer treatment. (4) Indeed, ICG has weak fluorescent emission. However, its fluorescence property has been directly used in certain clinical applications, and NIR fluorescence imaging using ICG has been reported.[30−34] Furthermore, its weak fluorescent emission should not overshadow its effect in photothermal therapy.
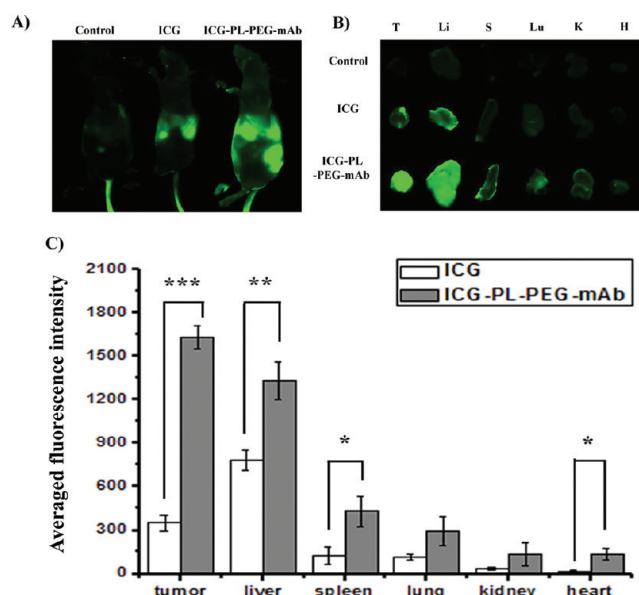
In our experiments, at an ICG concentration of 0.02 mg/mL, the ratio of monomer to dimer in ICG solution was 1.5, while in ICG-PL-PEG formulation, the ratio changed to 2.5 (Figure 1A). At an ICG concentration of 0.05 mg/mL, the ratio changed from 1.1 to 2.0 (data not shown). The monomer to dimer ratio in ICG-PL-PEG formulation was higher than that of ICG solution. It may be due to the noncovalent binding between ICG and PL-PEG as a strong competition to self-aggregation between ICG and ICG, which reduced the ICG
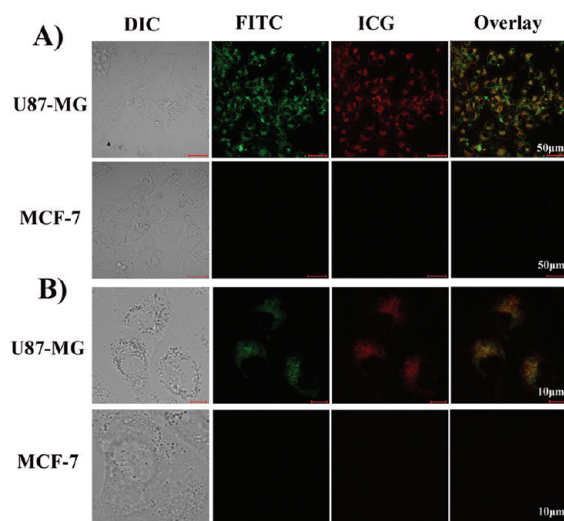
Figure 3. (A) Confocal images of U87-MG cells and MCF-7 cells after incubation in a solution of ICG-PL-PEG-mAb/FITC. U87-MG cells with overexpressed integrin $\alpha_v\beta_3$ show a high level of uptake of the targeting probe while MCF-7 cells with a low level of integrin $\alpha_v\beta_3$ show a low level of uptake. The fluorescence emissions from ICG (red) and FITC (green) were colocalized in U87-MG cancer cells, but absent in nontarget cells (MCF-7), which was clear evidence that ICG-PL-PEG-mAb/FITC remained stable after entering target cells. (B) High-magnification images of fluorescence emission from cells.


Figure 4. *In vivo* biodistribution analysis of ICG and ICG-PL-PEG-mAb. (A) The whole body NIR fluorescent images of mice were obtained six hours after intravenous injection. Detection was performed using the LI-COR Odyssey Infrared Imaging System through 800 nm channel (LI-COR, Inc. Lincoln, NE). ICG was mainly accumulated in liver, while ICG-PL-PEG-mAb had a high accumulation in both tumor and liver. (B) U87-MG tumor-bearing mice were sacrificed, and major organs were collected for fluorescence imaging. Spectrally resolved *ex vivo* fluorescence images of different organs were displayed. T: tumor. LI: liver. SP: spleen. LU: lung. K: kidney. H: heart. (C) Semiquantitative biodistribution of ICG and ICG-PL-PEG-mAb in mice determined by the averaged fluorescence intensity of each organ (after subtraction by the fluorescence intensity of each organ before injection). P values were calculated using nonpaired two-tailed Student's t test (*$P < 0.05$, **$P < 0.01$, ***$P < 0.001$; $n = 3$ per group).

dimerization. It is hypothesized that, due to the existence of two fatty acid acyls, PL-PEG contributes considerably to an increase in the van der Waals forces and hydrophobic interactions. However, further investigation is needed. The shift in wavelength of peak absorption was another evidence of the formation of ICG molecular aggregates between ICG and PL-PEG, which absorb and emit at longer wavelengths than the single ICG molecule. The red shifts have been previously reported in other delivery systems such as Solutol HS 15, Pluronic F-127, ICG-loaded PLGA nanoparticles, and nanoparticle assembled capsules.[32,41−43,45] Increased absorbance for ICG-PL-PEG for wavelength greater than 780 nm was due to the increase of ICG monomers. The absorption peak of the monomers is close to 800 nm, and this is the reason that the ICG-PL-PEG suspension was more efficient in producing a NIR-dependent temperature increase than aqueous ICG solution (Figure 1B).

In our *in vivo* experiments, the difference in temperature increase induced by ICG and ICG-PL-PEG was also due to their differential retentions in tumors, either through intratumoral injection (Figure 2E) or through intravenous injection (Figure 5C). It is well-known that ICG has a fast degradation rate in aqueous media and quick clearance from the body.[24,38−40] Due to its amphiphilic characteristics, ICG can interact with both lipophilic and hydrophilic molecules. In plasma, ICG binds almost completely (98%) to major plasma proteins, especially lipoproteins,[38] leading to its low vascular or tissue permeability. After binding to plasma proteins, ICG is excreted exclusively by liver, although the mechanism of ICG removal from blood is not clearly understand.[54] This behavior of ICG causes a rapid elimination from the bloodstream, with an initial half-life of 3−4 min, followed by a slower half-life of approximately 1 h at lower concentrations. All these properties lead to a low retention rate of ICG in tumor. Although the actual ICG content in the tumor was not calculated in this

study, the low averaged fluorescence intensity of ICG suggested a low retention of ICG in tumors (Figure 4), which was further supported by the data of temperature increase in tumors after laser irradiation (Figure 5C). Thus, ICG-PL-PEG provides ICG with chemical stability, protection from nonspecific protein binding, and enhanced circulation time.

When conjugated with a targeting antibody, ICG-PL-PEG could selectively enter tumor cells, as shown in Figure 3. This was further evidenced by the enhanced, prolonged fluorescent emission of ICG from the tumor, as shown in Figure 4, consistent with previous results using targeting lipid micelle as pharmaceutical carriers for poorly soluble drugs.[55−57] Due to the specific accumulation of ICG-PL-PEG-mAb in tumor, photothermal therapeutic effect could be achieved for tumor suppression, while laser + PBS or laser + ICG could provide only very limited impact on mouse tumors (Figure 5).

The stability and selective tumor uptake of ICG-PL-PEG made laser irradiation more effective at a late time point after the administration of ICG-PL-PEG and reduced the ICG binding in intravascular structure and in normal tissue. In this study, the laser irradiation took place six hours after ICG-PL-PEG administration. However, ICG-PL-PEG could be used as a dual-functional probe with integrated optical imaging and photothermal therapy capabilities. Therefore, the retention of ICG-PL-PEG in tumors could be used for tumor diagnosis through fluorescence imaging, and then the visualized tumor
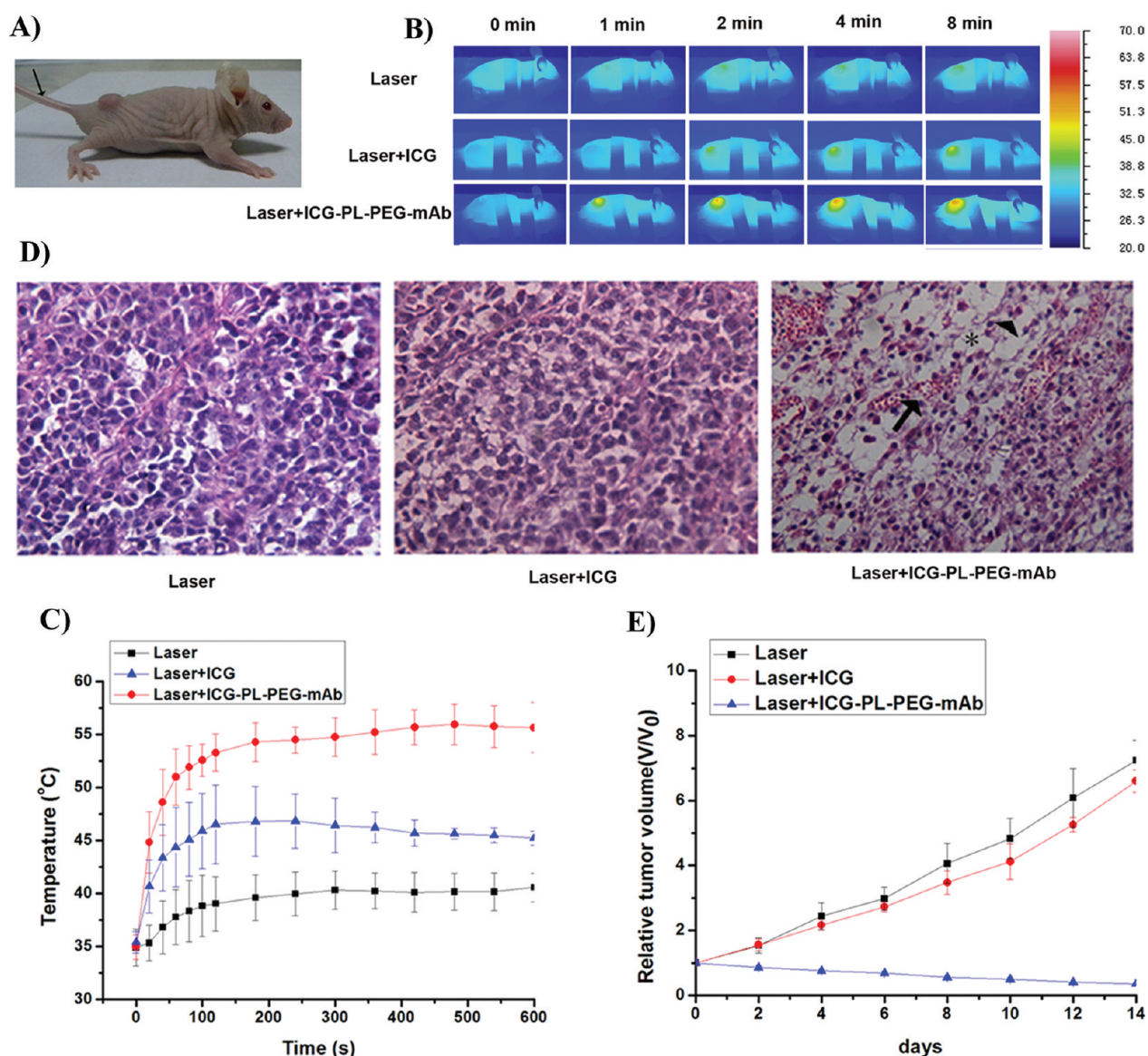
Figure 5. Photothermal treatment of mouse tumor using intravenous injection of ICG and ICG-PL-PEG-mAb, followed by laser irradiation. (A) Photograph of a mouse bearing U87-MG tumor. (B) Thermographic images of mice bearing U87-MG tumors under different treatments. (C) Plot of maximum surface temperature of the irradiated area as a function of the irradiation time ($n = 3$ per group). (D) Histological staining of the excised tumors 12 h after different treatments. Distinctive characteristics of cellular damage were observed in the laser + ICG-PL-PEG-mAb treated tumors, including coagulative necrosis (arrow), abundant pyknosis (arrowhead) and considerable regions of karyolysis (asterisk). (E) Time-dependent tumor growth curves of U87-MG tumor. The results were presented as the arithmetic means with standard deviations of tumor volumes in each group. Only the laser + ICG-PL-PEG-mAb treated group shows significant suppression of tumor growth compared with other experimental groups ($n = 3$).

could be destroyed with the 808 nm light in a noninvasive manner, while decreasing damage to the surrounding normal tissues. However, more appropriate time point will be optimized in our fluorescence work.

Nontargeting, sterically stabilized nanoparticles can extravasate into perivascular areas and adjacent extracellular space via enhanced permeability and retention (EPR) effect,[58−60] especially in tumors. However, most nontargeting nanostructures mainly accumulate in the interstitial space of the tumor and can be easily cleared. Therefore, attaching certain ligands, especially mAbs, as active targeting moieties onto these nanoparticles influences not only their specificity of the drug delivery but also their penetration and distribution in the tumor. Our results in this study demonstrated that ICG-PL-

PEG-mAb could effectively target tumor cells and increase their accumulation in tumors (Figure 3 and 4).

Nanotheranostics have attracted more and more attention recently, and multifunctional nanoparticles integrating imaging/detection and therapeutic capabilities are needed. NIR gold nanomaterials are limited in drug loading.[19] In contrast, organic nanoparticles, such as liposomes, micelles, and polymersomes, have found many human therapeutic applications as a result of their robust biocompatibility and drug-delivery capacity.[20] This unique ICG-PL-PEG, with integrated fluorescence imaging and photothermal therapeutic capabilities, can serve as dual-functional probes.[46]

CONCLUSION

To the best of our knowledge, this is the first report on *in vivo* photothermal effects using systemic administration of ICG-containing nanostructure. ICG-PL-PEG suspension was more efficient in producing a NIR-dependent temperature increase than ICG alone, due to the increase of ICG monomers from the addition of PL-PEG to match the central wavelength of the 808 nm laser. ICG-PL-PEG, when conjugated with monoclonal antibody (mAb), could be selectively internalized and retained in target tumor cells. Irradiation of an 808 nm laser after intravenous administration of ICG-PL-PEG-mAb resulted in tumor suppression in mice, while ICG alone had only a limited effect. Therefore, ICG-PL-PEG could be used as a fluorescent marker as well as a light-absorber for imaging-guided photothermal therapy.

AUTHOR INFORMATION

Corresponding Author

*South China Normal University, MOE Key Laboratory of Laser Life Science, Institute of Laser Life Science, Guangzhou 510631, China. Tel: (+86-20) 8521-0089. Fax: (+86-20) 8521-6052. E-mail: xingda@scnu.edu.cn.

Notes

The authors declare no competing financial interest.

ACKNOWLEDGMENTS

REFERENCES

(1) Nolsoe, C. P.; Torp-Pedersen, S.; Burcharth, F.; Horn, T.; Pedersen, S.; Christensen, N. E.; Olldag, E. S.; Andersen, P. H.; Karstrup, S.; Lorentzen, T.; et al. Interstitial hyperthermia of colorectal liver metastases with a US-guided Nd-YAG laser with a diffuser tip: a pilot clinical study. *Radiology* **1993**, *187*, 333–337.

(2) Amin, Z.; Donald, J. J.; Masters, A.; Kant, R.; Steger, A. C.; Bown, S. G.; Lees, W. R. Hepatic metastases: interstitial laser photocoagulation with real-time US monitoring and dynamic CT evaluation of treatment. *Radiology* **1993**, *187*, 339–347.

(3) Anghileri, L. J.; Robert, J. *Hyperthermia in Cancer Treatment*; CRC Press: Boca Raton, FL, 1986; pp 59–78.

(4) Weissleder, R. A clearer vision for in vivo imaging. *Nat. Biotechnol.* **2001**, *19*, 316–317.

(5) Chen, J.; Glaus, C.; Laforest, R.; Zhang, Q.; Yang, M.; Gidding, M.; Welch, M. J.; Xia, Y. Gold Nanocages as Photothermal Transducers for Cancer Treatment. *Small* **2010**, *6*, 811–817.

(6) Hirsch, L. R.; Stafford, R. J.; Bankson, J. A.; Sershen, S. R.; Rivera, B.; Price, R. E.; Hazle, J. D.; Halas, N. J.; West, J. L. Nanoshell-mediated near-infrared thermal therapy of tumors under magnetic resonance guidance. *Proc. Natl. Acad. Sci. U.S.A.* **2003**, *100*, 13549–13554.

(7) Dickerson, E. B.; Dreaden, E. C.; Huang, X.; El-Sayed, I. H.; Chu, H.; Pushpanketh, S.; McDonald, J. F.; El-Sayed, M. A. Gold nanorod assisted near-infrared plasmonic photothermal therapy (PPTT) of squamous cell carcinoma in mice. *Cancer Lett.* **2008**, *269*, 57–66.

(8) Jang, B.; Park, J. Y.; Tung, C. H.; Kim, I. H.; Choi, Y. Gold nanorod-photosensitizer complex for near-infrared fluorescence imaging and photodynamic/photothermal therapy in vivo. *ACS Nano* **2011**, *5*, 1086–1094.

(9) Choi, W. I.; Kim, J. Y.; Kang, C.; Byeon, C. C.; Kim, Y. H.; Tae, G. Tumor regression in vivo by photothermal therapy based on gold-nanorod-loaded, functional nanocarriers. *ACS Nano* **2011**, *5*, 1995–2003.

(10) Moon, H. K.; Lee, S. H.; Choi, H. C. In vivo near-infrared mediated tumor destruction by photothermal effect of carbon nanotubes. *ACS Nano* **2009**, *3*, 3707–3713.

(11) Zhou, F.; Xing, D.; Ou, Z.; Wu, B.; Resasco, D. E.; Chen, W. R. Cancer photothermal therapy in the near-infrared region by using single-walled carbon nanotubes. *J. Biomed. Opt.* **2009**, *14*, 021009.

(12) Yang, K.; Zhang, S.; Zhang, G.; Sun, X.; Lee, S. T.; Liu, Z. Graphene in mice: ultrahigh in vivo tumor uptake and efficient photothermal therapy. *Nano Lett.* **2010**, *10*, 3318–3323.

(13) Burke, A.; Ding, X.; Singh, R.; Kraft, R. A.; Levi-Polyachenko, N.; Rylander, M. N.; Szot, C.; Buchanan, C.; Whitney, J.; Fisher, J.; Hatcher, H. C.; D'Agostino, R. Jr.; Kock, N. D.; Ajayan, P. M.; Carroll, D. L.; Akman, S.; Torti, F. M.; Torti, S. V. Long-term survival following a single treatment of kidney tumors with multiwalled carbon nanotubes and near-infrared radiation. *Proc. Natl. Acad. Sci. U.S.A.* **2009**, *106*, 12897–12902.

(14) Zhang, M.; Murakami, T.; Ajima, K.; Tsuchida, K.; Sandanayaka, A. S.; Ito, O.; Iijima, S.; Yudasaka, M. Fabrication of ZnPc/protein nanohorns for double photodynamic and hyperthermic cancer phototherapy. *Proc. Natl. Acad. Sci. U.S.A.* **2008**, *105*, 14773–14778.

(15) Nel, A.; Xia, T.; Mädler, L.; Li, N. Toxic Potential of Materials at the Nanolevel. *Science* **2006**, *311*, 622–627.

(16) Lammers, T.; Kiessling, F.; Hennink, W. E.; Storm, G. Nanotheranostics and image-guided drug delivery: current concepts and future directions. *Mol. Pharmaceutics* **2010**, *7*, 1899–1912.

(17) Manthe, R. L.; Foy, S. P.; Krishnamurthy, N.; Sharma, B.; Labhasetwar, V. Tumor ablation and nanotechnology. *Mol. Pharmaceutics* **2010**, *7*, 1880–1898.

(18) Sun, D. Nanotheranostics: integration of imaging and targeted drug delivery. *Mol. Pharmaceutics* **2010**, *7*, 1879.

(19) Ghosh, P.; Han, G.; De, M.; Kim, C. K.; Rotello, V. M. Gold nanoparticles in delivery applications. *Adv. Drug Delivery Rev.* **2008**, *60*, 1307–1315.

(20) Peer, D.; Karp, J. M.; Hong, S.; Farokhzad, O. C.; Margalit, R.; Langer, R. Nanocarriers as an emerging platform for cancer therapy. *Nat. Nanotechnol.* **2007**, *2*, 751–760.

(21) Lovell, J. F.; Jin, C. S.; Huynh, E.; Jin, H.; Kim, C.; Rubinstein, J. L.; Chan, W. C.; Cao, W.; Wang, L. V.; Zheng, G. Porphysome nanovesicles generated by porphyrin bilayers for use as multimodal biophotonic contrast agents. *Nat. Mater.* **2011**, *10*, 324–332.

(22) Mordon, S.; Devoisselle, J. M.; Soulie-Begu, S.; Desmettre, T. Indocyanine green: physicochemical factors affecting its fluorescence in vivo. *Microvasc. Res.* **1998**, *55*, 146–152.

(23) Dzurinko, V. L.; Gurwood, A. S.; Price, J. R. Intravenous and indocyanine green angiography. *Optometry* **2004**, *75*, 743–755.

(24) Desmettre, T.; Devoisselle, J. M.; Mordon, S. Fluorescence properties and metabolic features of indocyanine green (ICG) as related to angiography. *Surv. Ophthalmol.* **2000**, *45*, 15–27.

(25) Chen, W. R.; Adams, R. L.; Bartels, K. E.; Nordquist, R. E. Chromophore-enhanced in vivo tumor cell destruction using an 808-nm diode laser. *Cancer Lett.* **1995**, *94*, 125–131.

(26) Chen, W. R.; Adams, R. L.; Heaton, S.; Dickey, D. T.; Bartels, K. E.; Nordquist, R. E. Chromophore-enhanced laser-tumor tissue photothermal interaction using an 808-nm diode laser. *Cancer Lett.* **1995**, *88*, 15–19.

(27) Chen, W. R.; Adams, R. L.; Higgins, A. K.; Bartels, K. E.; Nordquist, R. E. Photothermal effects on murine mammary tumors using indocyanine green and an 808-nm diode laser: an in vivo efficacy study. *Cancer Lett.* **1996**, *98*, 169–173.

(28) Chen, W. R.; Liu, H.; Ritchey, J. W.; Bartels, K. E.; Lucroy, M. D.; Nordquist, R. E. Effect of different components of laser immunotherapy in treatment of metastatic tumors in rats. *Cancer Res.* **2002**, *62*, 4295–4299.

(29) Chen, W. R.; Singhal, A. K.; Liu, H.; Nordquist, R. E. Antitumor immunity induced by laser immunotherapy and its adoptive transfer. *Cancer Res.* **2001**, *61*, 459−461.

(30) Altinoglu, E. I.; Russin, T. J.; Kaiser, J. M.; Barth, B. M.; Eklund, P. C.; Kester, M.; Adair, J. H. Near-infrared emitting fluorophore-doped calcium phosphate nanoparticles for in vivo imaging of human breast cancer. *ACS Nano* **2008**, *2*, 2075−2084.

(31) Ogawa, M.; Kosaka, N.; Choyke, P. L.; Kobayashi, H. In vivo molecular imaging of cancer with a quenching near-infrared fluorescent probe using conjugates of monoclonal antibodies and indocyanine green. *Cancer Res.* **2009**, *69*, 1268−1272.

(32) Kim, T. H.; Chen, Y.; Mount, C. W.; Gombotz, W. R.; Li, X.; Pun, S. H. Evaluation of temperature-sensitive, indocyanine green-encapsulating micelles for noninvasive near-infrared tumor imaging. *Pharm. Res.* **2010**, *27*, 1900−1913.

(33) Lee, C. H.; Cheng, S. H.; Wang, Y. J.; Chen, Y. C.; Chen, N. T.; Souris, J.; Chen, C. T.; Mou, C. Y.; Yang, C. S.; Lo, L. W. Near-Infrared Mesoporous Silica Nanoparticles for Optical Imaging: Characterization and In Vivo Biodistribution. *Adv. Funct. Mater.* **2009**, *19*, 215−222.

(34) Miki, K.; Oride, K.; Inoue, S.; Kuramochi, Y.; Nayak, R. R.; Matsuoka, H.; Harada, H.; Hiraoka, M.; Ohe, K. Ring-opening metathesis polymerization-based synthesis of polymeric nanoparticles for enhanced tumor imaging in vivo: Synergistic effect of folate-receptor targeting and PEGylation. *Biomaterials* **2010**, *31*, 934−942.

(35) Yaseen, M. A.; Yu, J.; Wong, M. S.; Anvari, B. Laser-induced heating of dextran-coated mesocapsules containing indocyanine green. *Biotechnol. Prog.* **2007**, *23*, 1431−1440.

(36) Yu, J.; Yaseen, M. A.; Anvari, B.; Wong, M. S. Synthesis of Near-Infrared-Absorbing Nanoparticle-Assembled Capsules. *Chem. Mater.* **2007**, *19*, 1277−1284.

(37) Yu, J.; Javier, D.; Yaseen, M. A.; Nitin, N.; Richards-Kortum, R.; Anvari, B.; Wong, M. S. Self-assembly synthesis, tumor cell targeting, and photothermal capabilities of antibody-coated indocyanine green nanocapsules. *J. Am. Chem. Soc.* **2010**, *132*, 1929−1938.

(38) Yoneya, S.; Saito, T.; Komatsu, Y.; Koyama, I.; Takahashi, K.; Duvoll-Young, J. Binding properties of indocyanine green in human blood. *Invest. Ophthalmol. Vis. Sci.* **1998**, *39*, 1286−1290.

(39) Landsman, M. L.; Kwant, G.; Mook, G. A.; Zijlstra, W. G. Light-absorbing properties, stability, and spectral stabilization of indocyanine green. *J. Appl. Physiol.* **1976**, *40*, 575−583.

(40) Saxena, V.; Sadoqi, M.; Shao, J. Degradation kinetics of indocyanine green in aqueous solution. *J. Pharm. Sci.* **2003**, *92*, 2090−2097.

(41) Rodriguez, V. B.; Henry, S. M.; Hoffman, A. S.; Stayton, P. S.; Li, X.; Pun, S. H. Encapsulation and stabilization of indocyanine green within poly(styrene-alt-maleic anhydride) block-poly(styrene) micelles for near-infrared imaging. *J. Biomed. Opt.* **2008**, *13*, 014025.

(42) Yaseen, M. A.; Yu, J.; Wong, M. S.; Anvari, B. Stability assessment of indocyanine green within dextran-coated mesocapsules by absorbance spectroscopy. *J. Biomed. Opt.* **2007**, *12*, 064031.

(43) Saxena, V.; Sadoqi, M.; Shao, J. Enhanced photo-stability, thermal-stability and aqueous-stability of indocyanine green in polymeric nanoparticulate systems. *J. Photochem. Photobiol., B* **2004**, *74*, 29−38.

(44) Devoisselle, J. M.; Soulié-Bégu, S.; Mordon, S.; Desmettre, T.; Maillols, H. A Preliminary Study of the In Vivo Behaviour of an Emulsion Formulation of Indocyanine Green. *Lasers Med. Sci.* **1998**, 279−282.

(45) Kirchherr, A. K.; Briel, A.; Mader, K. Stabilization of indocyanine green by encapsulation within micellar systems. *Mol. Pharmaceutics* **2009**, *6*, 480−491.

(46) Zheng, X.; Xing, D.; Zhou, F.; Wu, B.; Chen, W. R. Indocyanine green-containing nanostructure as near infrared dual-functional targeting probes for optical imaging and photothermal therapy. *Mol. Pharmaceutics* **2011**, *8*, 447−456.

(47) Ou, Z.; Wu, B.; Xing, D.; Zhou, F.; Wang, H.; Tang, Y. Functional single-walled carbon nanotubes based on an integrin alpha v beta 3 monoclonal antibody for highly efficient cancer cell targeting. *Nanotechnology* **2009**, *20*, 105102.

(48) Liu, Z.; Cai, W.; He, L.; Nakayamal, N.; Chen, K.; Sun, X.; Chen, X.; Dai, H. In vivo biodistribution and highly efficient tumour targeting of carbon nanotubes in mice. *Nat. Nanotechnol.* **2007**, *2*, 47−52.

(49) Cilesiz, I. Controlled temperature photothermal tissue welding. *J. Biomed. Opt.* **1999**, *4*, 327−336.

(50) De la Zerda, A.; Liu, Z.; Bodapati, S.; Teed, R.; Vaithilingam, S.; Khuri-Yakub, B. T.; Chen, X.; Dai, H.; Gambhir, S. S. Ultrahigh sensitivity carbon nanotube agents for photoacoustic molecular imaging in living mice. *Nano Lett.* **2010**, *10*, 2168−2172.

(51) Naylor, M. F.; Chen, W. R.; Teague, T. K.; Perry, L.; Nordquist, R. E. In Situ Photo Immunotherapy: A Tumor-Directed Treatment Modality for Melanoma. *Br. J. Dermatol.* **2006**, *155*, 1287−1292.

(52) Li, X. S.; Naylor, M. F.; Nordquist, R. E.; Teague, T. K.; Howard, C. A.; Murray, C.; Chen, W. R. In Situ Photoimmunotherapy for Late-stage Melanoma Patients: a Preliminary Study. *Cancer Biol. Ther.* **2010**, *10*, 1077−1214.

(53) Li, X. S.; Ferrel, G. L.; Guerra, M. C.; Hode, T.; Lunn, J. A.; Adalsteinsson, O.; Nordquist, R. E.; Liu, H.; Chen, W. R. Preliminary safety and efficacy results of laser immunotherapy for the treatment of metastatic breast cancer patients. *Photochem. Photobiol. Sci.* **2011**, *10*, 817−821.

(54) Cherrick, G. R.; Stein, S. W.; Leevy, C. M.; Davidson, C. S. Indocyanine green: observations on its physical properties, plasma decay, and hepatic extraction. *J. Clin. Invest.* **1960**, *39*, 592−600.

(55) Musacchio, T.; Laquintana, V.; Latrofa, A.; Trapani, G.; Torchilin, V. P. PEG-PE micelles loaded with paclitaxel and surface-modified by a PBR-ligand: synergistic anticancer effect. *Mol. Pharmaceutics* **2009**, *6*, 468−479.

(56) Wang, T.; Petrenko, V. A.; Torchilin, V. P. Paclitaxel-loaded polymeric micelles modified with MCF-7 cell-specific phage protein: enhanced binding to target cancer cells and increased cytotoxicity. *Mol. Pharmaceutics* **2010**, *7*, 1007−1014.

(57) Torchilin, V. P.; Lukyanov, A. N.; Gao, Z.; Papahadjopoulos-Sternberg, B. Immunomicelles: targeted pharmaceutical carriers for poorly soluble drugs. *Proc. Natl. Acad. Sci. U.S.A.* **2003**, *100*, 6039−6044.

(58) Allen, T. M.; Cullis, P. R. Drug delivery systems: entering the mainstream. *Science* **2004**, *303*, 1818−1822.

(59) Hobbs, S. K.; Monsky, W. L.; Yuan, F.; Roberts, W. G.; Griffith, L.; Torchilin, V. P.; Jain, R. K. Regulation of transport pathways in tumor vessels: role of tumor type and microenvironment. *Proc. Natl. Acad. Sci. U.S.A.* **1998**, *95*, 4607−4612.

(60) Brannon-Peppas, L.; Blanchette, J. O. Nanoparticle and targeted systems for cancer therapy. *Adv. Drug Delivery Rev.* **2004**, *56*, 1649−1659.